Optical conductivity of metal nanofilms and nanowires: The rectangular-box model

Valery P. Kurbatsky and Valentin V. Pogosov*
Department of Micro- and Nanoelectronics, Zaporozhye National Technical University, Zhukovsky Str. 64, Zaporozhye 69063, Ukraine
(Received 26 August 2009; revised manuscript received 24 February 2010; published 1 April 2010)

The conductivity tensor is introduced for the low-dimensional electron systems. Within the particle-in-a-box model and the diagonal response approximation, components of the conductivity tensor for a quasihomogeneous ultrathin metal film and wire are calculated under the assumption $d \cong \lambda_F$ (where d is the characteristic small dimension of the system, λ_F is the Fermi wavelength for bulk metal). We find the transmittance of ultrathin films and compare these results with available experimental data. The analytical estimations for the size dependence of the Fermi level are presented, and the oscillations of the Fermi energy in ultrathin films and wires are computed. Our results demonstrate the strong size and frequency dependences of the real and imaginary parts of the conductivity components in the infrared range. A sharp distinction of the results for Au and Pb is observed and explained by the difference in the relaxation time of these metals.

DOI: 10.1103/PhysRevB.81.155404 PACS number(s): 73.61.−r, 73.40.−c, 72.20.Dp

I. INTRODUCTION

Thin-film materials, in particular, metal films are used widely in modern technologies including electronics. As a rule, ultrathin films are fragmentized (the island films) and consist of flat islands connected with the thin threads channels.[1–3]

Experimental techniques allow the optical characteristics in the infrared (IR) range to be measured not only for thin films (see, for example, Refs. 4–15) but also for the specifically grown nanorods antennas of the micrometer length.[16–18]

In Ref. 7, the authors for the first time measured the infrared conductivity of Pb ultrathin films. A decrease in the conductivity of the films was explained by their granular structure. Subsequently, Tu *et al.*[9] measured the optical characteristics of metal films at a temperature of 10 K and revealed an anomalous optical transparency in the far-IR range. Pucci *et al.*[14] were the first to study the quantum size effects in the transmission spectra of lead thin films by IR spectroscopy. It should be noted that results of measurements have been usually interpreted by experimenters in the framework of the modified Drude theory. A theoretical analysis of optical properties of ultrathin films and wires is necessary, in particular, for the diagnostics of the nanostructure materials[19] in order to use them in microelectronics and nanoelectronics.[20]

The important feature of the metal one-dimensional (1D) and two-dimensional (2D) systems, films and wires, is an anisotropy of their electrical and optical properties caused by the size quantization. For this reason, the conductivity of the low-dimensional systems is represented by a tensor $\sigma_{\alpha\beta}(\mathbf{q},\omega)$ which, in particular, determines the optical absorption. The dissipation of energy of the plane monochromatic electromagnetic wave with the frequency ω and the wave vector $\mathbf{q}$ in unit volume per unit time for a nonmagnetic material is

$$Q(\mathbf{q},\omega) = \frac{1}{4}\sum_{\alpha,\beta}\{\sigma^*_{\alpha\beta}(\mathbf{q},\omega) + \sigma_{\beta\alpha}(\mathbf{q},\omega)\}E_\alpha E^*_\beta,$$

where $E_{\alpha,\beta}$ are the components of the electric field.[21] However, the only value directly measurable for an ultrathin film in IR range is the transmittance.

The purpose of this work is to calculate components of the conductivity tensor for quasihomogeneous ultrathin metal films and wires provided the condition $d \cong \lambda_F$ is satisfied. We use the Wood and Ashcroft approach[22] adapted to this case. The main advancement is the procedure of the accurate determination of the Fermi level for a film and a wire of such a thickness with taking into account the size oscillations. The transmittance of the ultrathin films is also calculated in order to compare theoretical results with experimental data.[4,5]

The oscillatory behavior of the Fermi energy in confined (2D) electron gas was studied for the first time by Sandomirskii.[23] Later calculations were performed for thin films, spheres, and wires.[24–34] In the present paper, in order to describe the Fermi-energy behavior in low-dimensional metallic systems we use an elementary one-particle analytical approach.[32]

II. CONDUCTIVITY TENSOR

A film of thickness L (or a wire of radius ρ_0) comparable in magnitude to the Fermi wavelength of an electron in an infinite metal ($\lambda_F^0 \approx 0.5$ nm) will be referred to as the ultrathin film or wire (see Fig. 1). The longitudinal sizes of the sample are assumed to be considerably larger than the film thickness: $L \ll a,b$ (or $\rho_0 \ll \mathcal{L}$ for wire), which leads to the pronounced quantization of the transverse component of the electron momentum. This results in the formation of subbands, i.e., groups of energy levels corresponding to the same value of the transverse momentum component.

A response of an electron gas to the electromagnetic field $\mathbf{E}=\mathbf{E}_0 \exp[i_0(\mathbf{qr}-\omega t)]$ may be determined in a linear approximation by the density-matrix technique.

For the induced current one can obtain,[22]

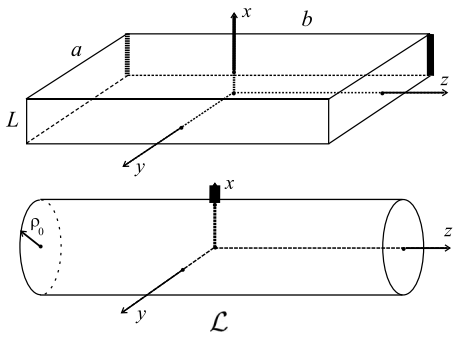

FIG. 1. Choice of coordinates.

$$\hat{\mathbf{j}}(\mathbf{k},\omega)=\frac{i_0e^2}{\Omega m_e\omega}\Bigg\{\mathbf{E}_0\sum_i f_i\langle i|e^{i_0(\mathbf{q}-\mathbf{k})\mathbf{r}}|i\rangle + \frac{1}{m_e}\sum_{ij}\frac{f_i-f_j}{\varepsilon_{ij}-\hbar w}\left(\langle j|e^{-i_0\mathbf{kr}}\hat{\mathbf{p}}|i\rangle-\frac{1}{2}\hbar\mathbf{k}\langle j|e^{-i_0\mathbf{kr}}|i\rangle\right) \times\left(\langle i|e^{i_0\mathbf{qr}}\mathbf{E}_0\hat{\mathbf{p}}|j\rangle+\frac{1}{2}\hbar\mathbf{q}\mathbf{E}_0\langle i|e^{i_0\mathbf{qr}}|j\rangle\right)\Bigg\}, \quad (1)$$

where $i_0=\sqrt{-1}$; $|i\rangle$, $|j\rangle$ are the wave functions of the initial and final electron states corresponding to energies ε_i and ε_j; $\varepsilon_{ij}=\varepsilon_i-\varepsilon_j$; f_j and f_j are occupation factors; Ω is the volume of sample, m_e is the electron mass, $-e$ is the electron charge, and $\hat{\mathbf{p}}$ is the momentum operator.

We describe conductivity electrons in metal films and wires within the framework of the particle-in-a-box model. In many cases, this model turns out to be quite productive for metals with high conductivity.[35] In the case of the low-dimensional electron systems, a potential box model includes the key feature of these systems—a confinement of electrons inside a region with certain small dimension. The model remains applicable up to a certain critical size when conductivity vanishes. As for the depth of a box, this parameter remains important as long as electron emitting is permitted.

In general, the model of electron gas in a rectangular potential box is a good initial approximation while various details (particularities of structure, impurities, etc.) can be taken into account by introducing corresponding corrections.

An electron system in low-dimensional structures is anisotropic and its characteristics can be expressed in tensor form. The tensor origin of the conductivity becomes obvious after converting the expression (1) into the form

$$j_\alpha(\mathbf{k},\omega)=\sum_\beta\sigma_{\alpha\beta}(\mathbf{k},\mathbf{q},\omega)E_\beta(\mathbf{q},\omega),$$

where α, $\beta=x,y,z$, and $\sigma_{\alpha\beta}$ is the conductivity tensor.

It is not difficult to demonstrate that the conductivity tensor is proportional to $\delta_{\alpha\beta}\delta_{\mathbf{k},\mathbf{q}}$, where $\delta_{\alpha\beta}$ or $\delta_{\mathbf{k},\mathbf{q}}=\{1,\mathbf{k}=\mathbf{q};\ 0,\mathbf{k}\neq\mathbf{q}\}$ is Kronecher's symbol, for macroscopic samples with the wave functions of the kind $\Omega^{-1/2}\exp(-\mathbf{pr}/\hbar)$. This implies that all the Fourier components of the current, except the one with $\mathbf{k}=\mathbf{q}$, are equal to zero. Of course, this is not the case for ultrathin films and wires but the component with $\mathbf{k}=\mathbf{q}$ is still dominating. At the first step, known as the diagonal response approximation, this component only is taken into account. We then find

$$\sigma_{\alpha\beta}(\mathbf{q},\mathbf{q},\omega)=\frac{i_0e^2N}{m_e\omega\Omega}\delta_{\alpha\beta}+\frac{i_0e^2}{m_e^2\omega\Omega}\sum_{i,j}\frac{f_i-f_j}{\varepsilon_{ij}-\hbar\omega} \times\left(\langle j|e^{-i_0\mathbf{qr}}\hat{p}_\alpha|i\rangle-\frac{1}{2}\hbar q_\alpha\langle j|e^{-i_0\mathbf{qr}}|i\rangle\right) \times\left(\langle i|e^{i_0\mathbf{qr}}\hat{p}_\beta|j\rangle+\frac{1}{2}\hbar q_\beta\langle i|e^{i_0\mathbf{qr}}|j\rangle\right) \equiv\sigma_{\alpha\beta}(\mathbf{q},\omega). \quad (2)$$

Here the relation $\Sigma_i f_i=N$ is used with N equal to the number of the conductivity electrons.

Over infrared region, the condition qL, $q\rho_0\ll 1$ is satisfied allowing us to express the conductivity tensor in terms of the according small value.

III. FILM

It is assumed that the conduction electrons of the film are located in a rectangular potential box $V(\mathbf{r})$ with a depth $U_0<0$, so that the box shape reproduces the film shape (see Fig. 1), and

$$|U_0|=\varepsilon_F^0+W_0,\quad \varepsilon_F^0=\frac{\hbar^2}{2m}(3\pi^2\bar{n})^{2/3}. \quad (3)$$

Here W_0, ε_F^0, and $\bar{n}$ are the electron work function, the Fermi energy, and the electron concentration for a bulk metal, respectively.

The unperturbed states of the film are described by the wave functions

$$\Psi_{mnp}(x,y,z)=\frac{1}{\sqrt{ab}}\psi_m(x)e^{2\pi ni_0y/a}e^{2\pi pi_0z/b}, \quad (4)$$

where $n,p=\pm1,\pm2,\ldots$ and $m=+1,+2,\ldots$. The subscript m numbers the subbands. The wave functions $\psi_m(x)$ are represented in the following form.

For even values of m,

$$\psi_m(x)=\begin{cases}C_m\sin k_{xm}x & -L/2<x<L/2\\ (-1)^{(m/2)+1}B_me^{-\kappa_mx} & x>L/2\\ (-1)^{m/2}B_me^{\kappa_mx} & x<-L/2,\end{cases} \quad (5)$$

and for odd values of m,

$$\psi_m(x)=\begin{cases}C_m\cos k_{xm}x & -L/2<x<L/2\\ (-1)^{(m-1)/2}B_me^{-\kappa_mx} & x>L/2\\ (-1)^{(m-1)/2}B_me^{\kappa_mx} & x<-L/2,\end{cases}$$

$$C_m=\sqrt{\frac{2\kappa_m}{2+\kappa_mL}},\quad B_m=C_m\frac{k_{xm}}{k_0}e^{\kappa_mL/2}. \quad (6)$$

Here, C_m is the normalization factor, k_{xm} are the roots of the equation

$$k_{xm}L=-2\arcsin(k_{xm}/k_0)+\pi m, \quad (7)$$

where $\kappa_m=\sqrt{k_0^2-k_{xm}^2}$ and $\hbar k_0=\sqrt{2m_e|U_0|}$ (see Ref. 32).

In this section, we focus on optical transitions between subbands accompanied by changing the transverse component of the electron wave vector k_{xm}. These transitions contribute to the σ_{xx} component of the conductivity tensor. Since $qL \ll 1$, we have in zero approximation

$$\sigma_{xx} = \frac{i_0 e^2}{m_e \omega \Omega}\left(N + \frac{1}{m_e}\sum_{i,j}\frac{f_i - f_j}{\varepsilon_{ij} - \hbar\omega}|\langle j|e^{-i_0(q_y y + q_z z)}\hat{p}_x|i\rangle|^2\right). \tag{8}$$

Dividing by $\varepsilon_{ij} - \hbar\omega$ in the sum and interchanging i and j for the second term appeared after this dividing, expression (8) can be transformed into

$$\sigma_{xx} = \frac{i_0 e^2}{m_e \omega \Omega}\left(N + \frac{2}{m_e}\sum_{i,j}\frac{f_i \varepsilon_{ij}}{\varepsilon_{ij}^2 - \hbar^2\omega^2}|\langle j|e^{-i_0(q_y y + q_z z)}\hat{p}_x|i\rangle|^2\right). \tag{9}$$

Since

$$\langle j|e^{-i_0(q_y y + q_z z)}\hat{p}_x|i\rangle = \langle m'|\hat{p}_x|m\rangle \delta_{q_y, k_{yn} - k_{yn'}} \delta_{q_z, k_{zp} - k_{zp'}},$$

and in view of the fact that $|k_{xm} - k_{xm'}| \gg q$, further simplifications are possible,

$$\sigma_{xx} \approx \frac{i_0 e^2}{m_e \omega \Omega}\left(N + \frac{2}{m_e}\sum_{\substack{m,m' \\ n,p}}\frac{f_{mnp}\varepsilon_{mm'}}{\varepsilon_{mm'}^2 - \hbar^2\omega^2}|\langle m'|\hat{p}_x|m\rangle|^2\right). \tag{10}$$

Here the occupation factor is approximated by the step function $f_{mnp} = \theta(\varepsilon_F - \varepsilon_{mnp})$, where ε_F is the Fermi energy for nanofilm, $\varepsilon_{mm'} = \hbar^2(k_{xm}^2 - k_{xm'}^2)/2m_e$. Using Thomas-Reiche-Kuhn sum rule (see Ref. 22), we rewrite Eq. (10) as

$$\sigma_{xx} = \frac{2 i_0 e^2 \hbar^2 \omega}{m_e^2 \Omega}\sum_{\substack{m,m' \\ n,p}}\frac{f_{mnp}|\langle m'|\hat{p}_x|m\rangle|^2}{\varepsilon_{mm'}(\varepsilon_{mm'}^2 - \hbar^2\omega^2)}, \tag{11}$$

and then one can obtain corresponding component of the dielectric tensor

$$\epsilon_{xx} = 1 + \frac{4\pi i_0}{\omega}\sigma_{xx}. \tag{12}$$

The matrix elements of the momentum projection operator $\hat{p}_x = i\hbar\,\partial/\partial x$ from Eqs. (4)–(6) are

$$|\langle m'|\hat{p}_x|m\rangle|^2 = \{1 - (-1)^{m+m'}\} \times \frac{8\hbar^2 k_{xm}^2 k_{xm'}^2 \kappa_m \kappa_{m'}}{(k_{xm'}^2 - k_{xm}^2)^2 (2 + \kappa_m L)(2 + \kappa_{m'} L)}. \tag{13}$$

The broadening is introduced in a manner proposed by Mermin.[36] As a result of this procedure the tensor components σ_{xx} and ϵ_{xx} get both real and imaginary parts,

$$\mathrm{Re}\ \sigma_{xx} = \left(\frac{4}{L}\right)^3 \frac{a_0 \gamma^2}{\pi}\left(\frac{1}{\hbar}\frac{e^2}{2a_0}\right) H_{(+)}, \tag{14}$$

$$\mathrm{Im}\ \sigma_{xx} = -\left(\frac{4}{L}\right)^3 \frac{a_0 k_\omega^2}{\pi}\left(\frac{1}{\hbar}\frac{e^2}{2a_0}\right) H_{(-)}, \tag{15}$$

$$\mathrm{Re}\ \epsilon_{xx} = 1 + \left(\frac{4}{L}\right)^4 \frac{L}{a_0} H_{(-)}, \quad \mathrm{Im}\ \epsilon_{xx} = \left(\frac{4}{L}\right)^4 \frac{L\gamma^2}{a_0 k_\omega^2} H_{(+)}, \tag{16}$$

where

$$H_{(\mp)} = \sum_{m=1}^{m_F}\sum_{m'=1}^{m_{\max}}[1 - (-1)^{m+m'}] \frac{L^2 \kappa_m \kappa_{m'} k_{xm}^2 k_{xm'}^2 (k_F^2 - k_{xm}^2)[(k_{xm'}^2 - k_{xm}^2)^2 \mp k_\omega^4 \mp \gamma^4]}{(2 + \kappa_m L)(2 + \kappa_{m'} L)(k_{xm'}^2 - k_{xm}^2)^3 \{[(k_{xm'}^2 - k_{xm}^2)^2 - k_\omega^4 + \gamma^4]^2 + 4k_\omega^4 \gamma^4\}}. \tag{17}$$

Here $\gamma = \sqrt{2m_e/\hbar\tau}$, τ is the relaxation time, $\hbar k_\omega = \sqrt{2m_e \hbar\omega}$, a_0 is the Bohr radius and

$$m_F = \left[\frac{L k_F}{\pi} + \frac{2}{\pi}\arcsin\left(\frac{k_F}{k_0}\right)\right], \quad m_{\max} = \left[\frac{L k_0}{\pi}\right] + 1. \tag{18}$$

Square brackets in Eq. (18) and in the text below indicate the integer number. Instead of the summation over n and p in Eqs. (11) and (12), we perform integration.

In order to use Eqs. (14)–(18) in calculations, it is necessary to supplement them by the relation determining the Fermi energy of film[32]

$$k_F^2 = \frac{1}{m_F}\left(2\pi\bar{n}L + \sum_{m=1}^{m_F} k_{xm}^2\right). \tag{19}$$

The relation (19) together with Eqs. (7) and (18) describes the size-dependent Fermi level in ultrathin films.

In the case of a film, transmittance is a quantity, which is directly measurable

$$\mathrm{TR} = I/I_0, \tag{20}$$

where I_0 and I are intensities of a wave at surfaces $x = -L/2$ and $x = L/2$, respectively.

For a film of thickness L the transmittance may be estimated as,

$$\mathrm{TR} = \exp\{-\eta(\omega,L)L\}, \tag{21}$$

where the absorption coefficient η should be calculated by using Eq. (16) and the formula

$$\eta = \frac{2\omega}{c}\mathrm{Im}\sqrt{\epsilon(\omega,L)}. \tag{22}$$

IV. WIRE

The simplest model for an ultrathin wire (see Fig. 1) is to consider it as a cylindrical potential well $V(\rho,z)$ of infinite depth. The length of the well $\mathcal{L}$ is assumed to be much larger than its radius ρ_0. The conductivity electrons are described by the wave functions of the kind

$$\psi_{mnp}(\rho,\varphi,z) = R_{mn}(\rho)\Phi_m(\varphi)\mathrm{Z}_p(z). \tag{23}$$

The function

$$\mathrm{Z}_p(z) = \frac{1}{\sqrt{\mathcal{L}}}e^{i_0 k_{zp} z} \tag{24}$$

corresponds to the longitudinal motion of an electron. The subscript p numbers values of z component of its wave vector. The angle part of the wave function

$$\Phi_m(\varphi) = \frac{1}{\sqrt{2\pi}}e^{i_0 m\varphi} \tag{25}$$

has to satisfy the periodicity condition

$$\Phi_m(\varphi + 2\pi) = \Phi_m(\varphi), \tag{26}$$

from which follows the eigenvalues spectrum $m = 0, \pm 1, \pm 2, \ldots$.

The radial dependence of the wave function is described by the Bessel functions of an integer order

$$R_{mn}(\rho) = C_{mn} I_m(k_{mn}\rho), \tag{27}$$

where

$$C_{mn} = \frac{\sqrt{2}}{\rho_0 |I'_m(k_{mn}\rho_0)|}. \tag{28}$$

Here $k_{mn} = a_{mn}/\rho_0$, where a_{mn} are positive roots of the Bessel function of the mth order $I_m(\xi)$, $n = 1, 2, \ldots$. The prime marks a derivative with respect to ξ.

In the next section, for the case of a wire, we obtain the relation similar to Eq. (19).

A. Fermi energy

We start from the expression for the energy of an electron

$$\varepsilon_{mnp} = \frac{\hbar^2}{2m_e}(k_{mn}^2 + k_{zp}^2), \tag{29}$$

where k_{mn} and k_{zp} are the eigenvalues of transverse and longitudinal components of the electron wave vector, respectively.[20] The electron states in a wire correspond to points (k_{mn}, k_{zp}) on the $k_\perp$ k_{zp} half plane $(k_\perp > 0)$. Since the spectrum k_{zp} is quasicontinuous $(\mathcal{L} \gg \rho_0)$, these points form a system of straight lines $k_\perp = k_{mn}$. The occupied states distribute on intercepts cutoff by the semicircle of radius k_F (see Fig. 2). Density of the electron states at the intercepts is equal to $\mathcal{L}/\pi$.

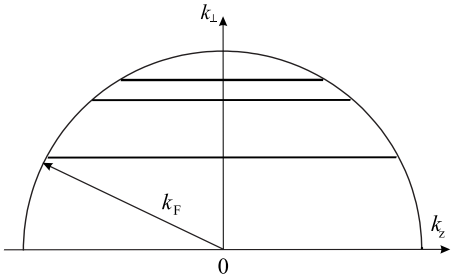

FIG. 2. Geometrical diagram of electron-state filling in quantum wire.

The total number of the occupied states (equal to the number of the conduction electrons in a wire) is

$$N = 2\frac{\mathcal{L}}{\pi}\sum_{m,n}\sqrt{k_\mathrm{F}^2 - k_{mn}^2}.$$

Taking into account that $N = \bar{n}\Omega$, we then obtain the equation for the computation of the Fermi level k_F in an ultrathin wire

$$\bar{n} = \frac{2}{\pi^2\rho_0^2}\sum_{m,n}\sqrt{k_\mathrm{F}^2 - k_{mn}^2}. \tag{30}$$

The electron concentration $\bar{n}$ is assumed to be the same in a wire and in a bulk metal. The summation should be performed over all numbers m and n satisfying the condition

$$k_{mn} \le k_\mathrm{F}. \tag{31}$$

The size dependence of the Fermi level in ultrathin films and wires has an "oscillatory" form. In order to determine a magnitude of the variations, let us evaluate the averaged (smoothed) size dependence. In this case, an averaging means a replacement of summation in Eqs. (19) and (30) by integration.

For a film, we use the Euler-MacLaurin summation formula,[37] in which it is enough to take into account the first two terms. Allowing m_F to take any value (not only integer, $m_\mathrm{F} \approx Lk_\mathrm{F}/\pi$) and neglecting the corrections for a finite depth of a potential box, we obtain

$$k_\mathrm{F}/k_\mathrm{F}^0 \approx 1 + \pi/(4k_\mathrm{F}^0 L), \tag{32}$$

where k_F^0 is the Fermi wave number for a bulk metal.

In the case of a wire, it is hard to estimate directly the size dependence of the Fermi level because it is impossible to express explicitly the roots of the Bessel functions. However, the averaged size dependence $k_\mathrm{F}(\rho_0)$ can be obtained in an indirect way.

Let us rewrite Eq. (30) as

$$(k_\mathrm{F}^0\rho_0)^3 = 6\sum_{m,n}\sqrt{(k_\mathrm{F}^0\rho_0)^2 - a_{mn}^2}.$$

Here $k_\mathrm{F}^0 = (3\pi^2\bar{n})^{1/3}$ and the relation

$$k_{mn} = a_{mn}/\rho_0 \tag{33}$$

was used. a_{mn} are positive roots of the Bessel function of order $m=0, \pm 1, \pm 2, \ldots$ and $n=1,2,\ldots$. Assuming the $a_{mn} = a(m,n)$ function to be continuous, we turn to the integration,

$$(k_F^0\rho_0)^3 = 12\int\int \sqrt{(k_F\rho_0)^2 - a^2(m,n)}dmdn \tag{34}$$

($m \geq 0$ now). Limits of the integration are determined by the condition $a(m,n) \leq k_F\rho_0$.

The left-hand side of Eq. (34) tends to zero with $\rho_0 \to 0$. At the same time, the right-hand side tends to zero only if $k_F\rho_0 \to a_{01}$. Hence, the averaged size dependence is

$$k_F(\rho_0) \approx a_{01}/\rho_0$$

for the small values ρ_0. For the large values ρ_0, the integrated expression is $k_F\rho_0$ and the area of the region of integration $\int\int dmdn$ is proportional to $k_F^2\rho_0^2$. Then, comparing the left-hand and right-hand sides, we find that $k_F(\rho_0) \to$ const with $\rho_0 \to \infty$. Accepting the constant to be k_F^0, we finally obtain

$$k_F/k_F^0 = 1 + a_{01}/(k_F^0\rho_0),$$

where $a_{01} \approx 2.4048$.

In Sec. IV B, to calculate conductivity components, we use the size-dependent Fermi energy ε_F found from the exact expression (30).

B. Components of the conductivity tensor

Let us consider the case when a wave is directed normally to the axis of a wire (see Fig. 1). The wave vector is then located in the x-y plane, i.e., $q_z=0$. Orientating the x axis along the wave propagation, we get $q_y=0$, $\mathbf{qr} = q_x x \simeq \rho_0/\lambda \ll 1$, and $e^{\pm i_0 \mathbf{qr}} \approx 1 \pm i_0 q_x x$.

In zero order of the expansion $\sigma_{\alpha\beta}$ in terms of ρ_0/λ, the expression (2) takes the form

$$\sigma_{\alpha\beta} = \frac{i_0 e^2 N}{m_e \omega \Omega}\delta_{\alpha\beta} + \frac{i_0 e^2}{m_e^2 \omega \Omega}\sum_{i,j}\frac{f_i - f_j}{\varepsilon_{ij} - \hbar\omega}\langle j|\hat{p}_\alpha|i\rangle\langle i|\hat{p}_\beta|j\rangle. \tag{35}$$

Following the procedure, which led us to Eq. (9), we have

$$\sigma_{\alpha\beta} = \frac{i_0 e^2 N}{m_e \omega \Omega}\delta_{\alpha\beta} + \frac{i_0 e^2}{m_e^2 \omega \Omega}\sum_{i,j} f_i \times \left(\frac{\langle j|\hat{p}_\alpha|i\rangle\langle i|\hat{p}_\beta|j\rangle}{\varepsilon_{ij} - \hbar\omega} + \frac{\langle j|\hat{p}_\alpha|i\rangle^*\langle i|\hat{p}_\beta|j\rangle^*}{\varepsilon_{ij} + \hbar\omega}\right). \tag{36}$$

Using Eqs. (24)–(28), after rather cumbersome transformations (see Appendix), the matrix elements of various projections of the momentum operator can be written as

$$\langle j|\hat{p}_\alpha|i\rangle = \begin{cases} \hbar k_{zp}\delta_{ij} & \alpha = z \\ -\dfrac{i_0\hbar}{2}\delta_{pp'}k_{mn}C_{mn}\mathcal{G}_{(-)} & \alpha = x \\ \dfrac{\hbar}{2}\delta_{pp'}k_{mn}C_{mn}\mathcal{G}_{(+)} & \alpha = y; \end{cases} \tag{37}$$

$$\mathcal{G}_{(\mp)} = \delta_{m-1,m'}\mathcal{J}_{(-)} \mp \delta_{m+1,m'}\mathcal{J}_{(+)},$$

$$\mathcal{J}_{(\mp)} = C_{m\mp1,n'}\int_0^{\rho_0} I_{m\mp1}(k_{m\mp1,n'}\rho)I_{m\mp1}(k_{mn}\rho)\rho d\rho. \tag{38}$$

Because of a specific form of $\langle j|\hat{p}_z|i\rangle$ the sum in Eq. (35) becomes zero if $\alpha=z$ or $\beta=z$. Hence,

$$\sigma_{xz,zx,yz,zy} = 0, \quad \sigma_{zz} = \frac{i_0 e^2 \bar{n}}{m_e \omega}. \tag{39}$$

For other diagonal components, the expression (36) can be easily transformed into

$$\sigma_{\alpha\alpha} = \frac{i_0 e^2 \bar{n}}{m_e \omega} + \frac{2 i_0 e^2}{m_e^2 \omega \Omega}\sum_{i,j}\frac{f_i \varepsilon_{ij}}{\varepsilon_{ij}^2 - \hbar^2\omega^2}|\langle j|\hat{p}_\alpha|i\rangle|^2, \tag{40}$$

where the subscript $\alpha = x, y$. After a substitution of the matrix elements, Eq. (37), into Eq. (40), we find

$$\sigma_{xx,yy} = \frac{i_0 e^2 \bar{n}}{m_e \omega} + \frac{i_0 e^2}{m_e \omega \Omega}\sum_{m,n}{}^{p,n'} f_{mnp} k_{mn}^2 C_{mn}^2 \times \left\{\frac{(k_{mn}^2 - k_{m-1,n'}^2)\mathcal{J}_{(-)}^2}{(k_{mn}^2 - k_{m-1,n'}^2)^2 - k_\omega^4} + \frac{(k_{mn}^2 - k_{m+1,n'}^2)\mathcal{J}_{(+)}^2}{(k_{mn}^2 - k_{m+1,n'}^2)^2 - k_\omega^4}\right\}, \tag{41}$$

where

$$f_{mnp} = \begin{cases} 1 & k_{mn}^2 + k_{zp}^2 < k_F^2 \\ 0 & k_{mn}^2 + k_{zp}^2 > k_F^2. \end{cases}$$

An expression for the nondiagonal components σ_{xy} and σ_{yx} follows from Eq. (36),

$$\sigma_{\alpha\beta} = \frac{i_0 e^2}{m_e^2 \omega \Omega}\sum_{i,j} f_i \left(\frac{\langle j|\hat{p}_x|i\rangle\langle i|\hat{p}_y|j\rangle}{\varepsilon_{ij} \mp \hbar\omega} + \frac{\langle j|\hat{p}_x|i\rangle^*\langle i|\hat{p}_y|j\rangle^*}{\varepsilon_{ij} \pm \hbar\omega}\right). \tag{42}$$

The upper sign corresponds to $\alpha=x$, $\beta=y$, and the lower one to $\alpha=y$, $\beta=x$.

The axis symmetry of the problem is reflected by the fact that in Eqs. (35) and (36) the summation is performed over positive m and m' as well as negative ones but the same in absolute value. The analysis of the expressions (37) and (38) based on the properties of the Bessel functions[38]

$$k_{(-m)n} = k_{mn}, \quad I_{-m}(\xi) = (-1)^m I_m(\xi)$$

reveals a different behavior of the matrix elements when changing together $m \to -m$ and $m' \to -m'$,

$$\langle j|\hat{p}_x|i\rangle \to -\langle j|\hat{p}_x|i\rangle, \quad \langle j|\hat{p}_y|i\rangle \to \langle j|\hat{p}_y|i\rangle. \tag{43}$$

This causes the terms in Eq. (42) to cancel pairwise, and we then find

$$\sigma_{xy} = \sigma_{yx} = 0. \tag{44}$$

Thus, all nondiagonal components of the conductivity tensor vanish in zero approximation of the expansion in terms of

ρ_0/λ. However, in linear approximation the result is different. We take account that terms, which contain δ_{ij}, lead to the vanishing of the sum. Therefore, in this approximation, components σ_{zx} and σ_{zy} have a form

$$\sigma_{z\beta} = \frac{q_x e^2}{m_e^2 \omega \Omega} \sum_{i,j} f_i \left(\frac{\langle j|x\hat{p}_z|i\rangle\langle i|\hat{p}_\beta|j\rangle}{\varepsilon_{ij} - \hbar\omega} + \frac{\langle j|x\hat{p}_z|i\rangle^*\langle i|\hat{p}_\beta|j\rangle^*}{\varepsilon_{ij} + \hbar\omega} \right), \tag{45}$$

where $\beta = x, y$ and for the matrix elements see Appendix.

An analysis, similar to the one, which resulted in Eq. (43), gives

$$\langle j|x\hat{p}_z|i\rangle \to -\langle j|x\hat{p}_z|i\rangle, \quad \langle j|x\hat{p}_z|i\rangle\langle i|\hat{p}_y|j\rangle \to -\langle j|x\hat{p}_z|i\rangle \times\langle i|\hat{p}_y|j\rangle, \quad \langle j|x\hat{p}_z|i\rangle\langle i|\hat{p}_x|j\rangle \to \langle j|x\hat{p}_z|i\rangle\langle i|\hat{p}_x|j\rangle. \tag{46}$$

Hence, to linear order in ρ_0/λ we have $\sigma_{zy}=0$ but $\sigma_{zx}\neq 0$. Using Eq. (38), the relation

$$\langle j|x\hat{p}_z|i\rangle^*\langle i|\hat{p}_x|j\rangle^* = -\langle j|x\hat{p}_z|i\rangle\langle i|\hat{p}_x|j\rangle$$

and Eq. (A3), we derive

$$\sigma_{zx} = \frac{2i_0 q_x e^2}{\hbar\Omega} \sum_{\substack{n,n' \\ m,p}} f_{mnp} k_{zp} C_{mn}^2 (\mathcal{F}_{(-)} - \mathcal{F}_{(+)}), \tag{47}$$

where

$$\mathcal{F}_{(\mp)} = \frac{\mathcal{J}_{(\mp)} C_{m\mp 1,n'} \int_0^{\rho_0} I_{m\mp 1}(k_{m\mp 1,n'}\rho) I_m(k_{mn}\rho)\rho^2 d\rho}{(k_{mn}^2 - k_{m\mp 1,n'}^2)^2 - k_\omega^4}.$$

Dissipation is introduced by the substitution $\omega \to \omega + i_0/\tau$ in expression for conductivity. When $\tau=0$, the diagonal components of conductivity are imaginary. Since the remaining components of the tensor vanish in zero approximation, dissipation is also absent ($Q=0$). In general, dissipation is small for optical frequencies in which we are interested ($\omega \gg 1/\tau$).

Substituting $\omega \to \omega + i_0/\tau$ in Eq. (39), after straightforward transformations we obtain the Drude formula[39]

$$\sigma_{zz}(\omega) = \sigma(0)\frac{1 + i_0\omega\tau}{1 + \omega^2\tau^2}, \tag{48}$$

where $\sigma(0) \equiv e^2\bar{n}\tau/m_e$ is the static conductivity. Thus, the component $\sigma_{zz}(\omega)$ is associated with the classical conductivity. Other diagonal components, Eq. (40), can be represented as

$$\sigma_{\alpha\alpha} = \sigma_{zz}\{1 + S(\omega, \rho_0, \mathcal{L})\}, \tag{49}$$

where

$$S \equiv \frac{2}{Nm_e} \sum_{i,j} \frac{f_i \varepsilon_{ij}(\varepsilon_{ij}^2 - \hbar^2\omega^2 + 2\hbar^2\omega i_0/\tau)}{(\varepsilon_{ij}^2 - \hbar^2\omega^2)^2 + 4\hbar^4\omega^2/\tau^2} |\langle j|\hat{p}_\alpha|i\rangle|^2 \tag{50}$$

and $\alpha = x, y$.

After interchanging subscripts i and j, terms of the sum, Eq. (50), reverse their sign. As a result,

$$\sum_{\substack{i,j \\ \varepsilon_i,\varepsilon_j<\varepsilon_F}} \frac{f_i \varepsilon_{ij}(\varepsilon_{ij}^2 - \hbar^2\omega^2 + 2\hbar^2\omega i_0/\tau)}{(\varepsilon_{ij}^2 - \hbar^2\omega^2)^2 + 4\hbar^4\omega^2/\tau^2} |\langle j|\hat{p}_\alpha|i\rangle|^2 = 0$$

and

$$S = \frac{2}{Nm_e} \sum_{\substack{i,j \\ \varepsilon_i<\varepsilon_F \\ \varepsilon_j>\varepsilon_F}} \frac{\varepsilon_{ij}(\varepsilon_{ij}^2 - \hbar^2\omega^2 + 2\hbar^2\omega i_0/\tau)}{(\varepsilon_{ij}^2 - \hbar^2\omega^2)^2 + 4\hbar^4\omega^2/\tau^2} |\langle j|\hat{p}_\alpha|i\rangle|^2. \tag{51}$$

Here $\varepsilon_{ij}<0$, i.e., only transitions coupled with absorption participate in the conductivity. It is important to remark that Im $S<0$ for any frequency. Since in the optical region the real part of the component σ_{zz} can be ignored and its imaginary part is positive, it follows from Eq. (49) that Re $\sigma_{xx,yy}>0$ and $Q>0$ over the whole region.

Let us compare in magnitude components of the conductivity tensor. For Au, the frequency $\hbar\omega=1$ eV, dissipation $\hbar/\tau=0.02$ eV we find $\sigma(0)=4.6\times 10^{17}$ s^{-1}, $|\sigma_{zz}| \approx \sigma(0)/\omega\tau \approx 10^{16}$ s^{-1}. We use below the value $e^2/2a_0\hbar = 2.0\times 10^{16}$ s^{-1} as a unit of the conductivity. Then $|\sigma_{zz}| \approx 0.5$.

We can now estimate, for example, height of peaks in Re σ_{xx}. We use relationships

$$\text{Re } \sigma_{xx} = -|\sigma_{zz}|\text{Im } S$$

and

$$\text{Im } S \approx -\frac{\tau}{\hbar N m_e} |\langle m+1, n'|\hat{p}_x|mn\rangle|^2 \sum_p 1$$

[which may be obtained from Eqs. (49) and (50) under condition that the peaks are well separated]. Taking into account that

$$\sum_p 1 = \frac{2\mathcal{L}}{\pi}\sqrt{k_F^2 - k_{mn}^2} \cong \frac{2\mathcal{L}}{\pi} k_F^0, \tag{52}$$

$$|\langle m+1, n'|\hat{p}_x|mn\rangle|^2 \propto k_{mn}^2 \cong \frac{1}{4}\hbar^2 k_F^{0^2} \tag{53}$$

and, using Eq. (3), we have

$$\text{Im } S \cong -\frac{3\hbar\tau}{2m_e\rho_0^2}.$$

For $\tau=2.1\times 10^{-14}$ s^{-1} (Au), $d=2\rho_0=2$ nm, we find Im $S\cong -1$, Re $\sigma_{xx}\cong 1$. In macroscopic limit $\rho_0 \to \infty$ we find that Re $\sigma_{xx}=0$ and Im $\sigma_{xx}=$Im σ_{zz}, as we have expected.

Comparing Eq. (36) with Eq. (45), one can obtain $|\sigma_{zx}/\sigma_{xx}| \cong q_x\rho_0$. For $\lambda=10^3$ nm, $d=2$ nm we have $|\sigma_{zx}/\sigma_{xx}| \cong 10^{-2}$.

V. RESULTS AND DISCUSSION

The difference between our approach and the theory[22] is associated with peculiarities of an electronic levels distribu-

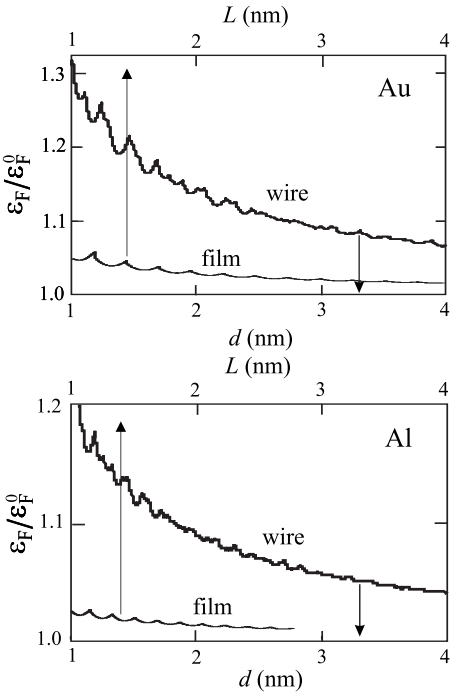

FIG. 3. Reduced size dependences of the Fermi energy of wires and films vs diameter $d=2\rho_0$ and thickness L, respectively.

tion in films/wires of nanometers thickness, when the $d \cong \lambda_F$ condition is satisfied.

In this case, a number of subbands, formed as a result of the size quantization, is small, while the contribution of each of them in the sum, Eq. (17), is significant. Opposite assumptions are made in Ref. 22: a characteristic size d is so large that the number of subbands is much larger than 1. Then, the separation between neighboring subbands (with numbers m and $m+1$) is small, while contributions of individual items in the sum[22] are not significant anymore, so the summation can be substituted by integration, as usually done in the case of a quasicontinuous distribution. Discreteness, coming from the size quantization, manifests itself only weakly. The Fermi level in films and wires with small thickness noticeably differs from the Fermi level of a bulk metal (30% difference for a wire of 1 nm diameter, see Fig. 3). In Ref. 22, the authors use the Fermi level of a bulk metal to find a number of subbands, while we take into account the size dependence of the Fermi level, when determining a number of subbands. For a few nanometers thickness, these numbers are found to be different and, because they are small, a noticeable divergence in results is revealed.

Finally, theory[22] was developed in order to apply it for an isotropic composite medium. Therefore, from the very beginning, the direction of an applied field was considered as a preferred one. In our approach, anisotropy of the metallic 1D and 2D systems (wires and films) is taken into consideration, their conductivity and dielectric function are assumed to be tensors that allows a response of wires and films to be determined for any orientation in an external field.

Anisotropy as well as discreteness manifests itself much stronger in systems with the small characteristic size $d \cong \lambda_F$. Under the condition $d \gg \lambda_F$, both our theory and theory[22] lead to the same results.

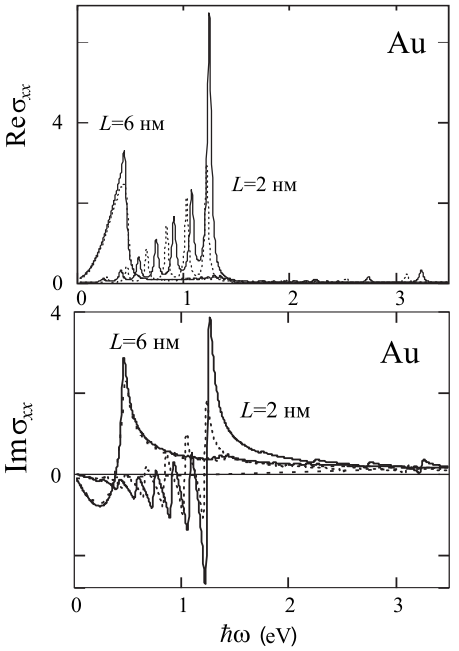

FIG. 4. Frequency dependences of the real and imaginary parts of the film conductivity component (in $e^2/2a_0\hbar$ units) calculated by Eqs. (14) and (15) (solid lines). Dashed curves correspond to the results of calculations by formula (68) from work (Ref. 22).

A. Fermi energy

Figure 3 demonstrates the size dependence of the Fermi energy for films and wires of Au and Al computed from Eqs. (19) and (30). The size dependences have an "oscillatory" form. In contrast to the Fermi energy of a film,[32] the size variation in the Fermi energy of a wire seems to be random. Input parameters for calculations were taken from Ref. 32.

In the case of a film, cusps on the size dependence (i.e., the jumps of the derivative $d\varepsilon_F/dL$) are distributed nearly regular with the approximately constant period $\Delta L \approx \pi/k_F^0$. The cusp on the size dependence of a wire appears each time when the increasing radius ρ_0 reaches the value $\rho_{0(m'n')}$ for which the condition (31) is satisfied by one more pair (m',n'),

$$a_{m'n'} = k_F \rho_{0(m'n')}.$$

Distance between the neighboring cusps is

$$\Delta d \approx 2(a_{m'n'} - a_{mn})/k_F^0,$$

where a_{mn} is the root of the Bessel function closest to $a_{m'n'}$ in value. Roots of the Bessel functions of different orders mix up so that Δd varies, at first sight, randomly with change in size.

The oscillations of the Fermi energy in a wire of diameter d and in a film of thickness L are similar in magnitude if $d \cong L$. As in the case of a film, the "period" Δd and the amplitude of the oscillations tend to zero with increasing diameter.

Characteristic properties of the size dependence of the Fermi energy for various metal wires (and various metal

films too) may be explained exclusively by different value k_F^0. As compared to the Au wire, for the Al wire, the scale Δd of the oscillations is finer, the amplitude of the oscillations and the averaged value $\varepsilon_F/\varepsilon_F^0$ are smaller.

B. Film

The specific feature of the optical characteristics of thin films is the presence of peaks associated with the optical transitions between the subbands. The size effect manifests itself in a change in the number of peaks, their position, and the spacing between them.

The positions of the peaks is determined by the approximate expression $\hbar\omega_{mm'} \approx \hbar\omega_0|m'^2 - m^2|$, where m and m' are the numbers of subbands between which the transition occurs and $\hbar\omega_0 \equiv \pi^2\hbar^2/(2m_eL^2) = 0.34\ [\text{eV}]/L^2\ [\text{nm}^2]$. The frequency range under consideration lies in the infrared and visible spectral ranges. The lower limit of the range ($\hbar\omega_{12}$) corresponds to the beginning of the optical transitions between the subbands. The upper limit of the frequency range is the electron work function W of the film. The estimates can be made with the work function W_0 for infinite metals Au and Ag.

The calculated real and imaginary parts of the conductivity component σ_{xx} for the Au films 2 and 6 nm thick are presented in Fig. 4. For ultrathin films, the number of subbands completely or partially occupied by electrons is small: $m_F \approx 2L/\lambda_F^0$. Therefore, the number of peaks is small as well. For the film of the thickness $L=2$ nm, the peak at $\hbar\omega_{12} \approx 0.25$ eV corresponding to the lower limit of the frequency range is clearly seen. The peaks that represent the transitions between the neighboring subbands with the numbers m and $m'=m+1$ are located to the left of the maximum height peak observed at the frequency $\hbar\omega_{\max} \simeq \hbar\omega_0(2m_F+1)$. This frequency corresponds to the transition between the subbands with the numbers $m=m_F$ and $m'=m_F+1$. The spacing between any two neighboring peaks is identical and approximately equal to $2\hbar\omega_c$. As the film thickness L increases, all peaks shift toward the left, the spacing between peaks decreases, and they begin to merge together.

The overlapping of the peaks becomes significant when the spacing between them is equal to their width. The peak width is determined by the dissipation mechanisms and is approximately equal to $2\hbar/\tau$. Peaks for the film of the thickness $L=2$ nm are clearly distinguishable (see Fig. 4) but for the thickness $L=6$ nm the peaks disappear completely. (It should be noted that the results of our calculations appear to be weakly sensitive to a change in the relaxation time τ within 1 order of magnitude.)

It can be seen from Fig. 4 that, as the film thickness decreases, the discrepancy between the results of calculations by Eqs. (14) and (15) and by Eq. (68) from Ref. 22 increases and becomes substantial. This discrepancy is associated with the fact that relationships, Eqs. (14) and (15), were derived with allowance made for the dependence of the Fermi energy on the film thickness $k_F(L)$ and the exact calculation of the number m_F of occupied subbands. In Ref. 22, the number m_F was calculated by the procedure which gives an error ± 1 for films with thickness $L \simeq \lambda_F$. This is an essential error because the number of occupied subbands for such thickness is small and ranges from 2 to 6.

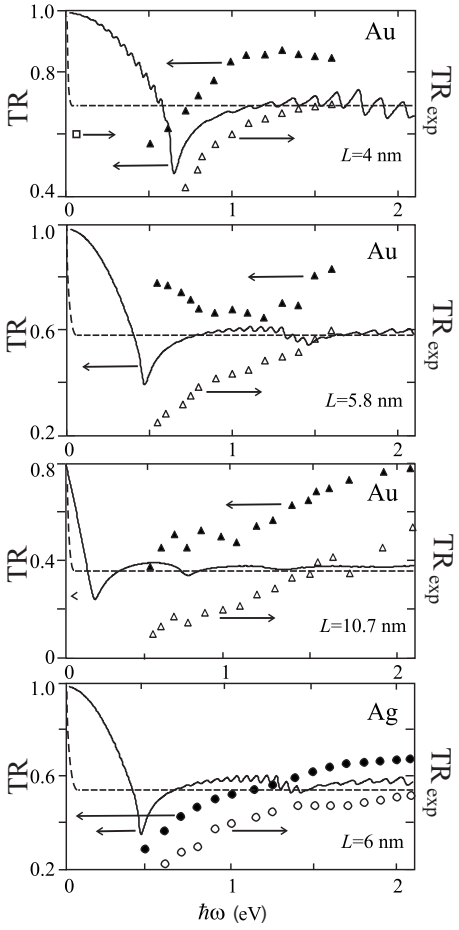

FIG. 5. Frequency dependences of the film transmittance calculated by Eqs. (14)–(22) using ϵ_{xx} (solid lines) and ϵ_{zz} (dashed lines, left-hand scale). Opened triangles (Ref. 5), circles (Ref. 4), and square (Ref. 9) indicate the experimental data (right-hand scale) for the Au and Ag films. Solid triangles and circles indicate the recalculated experimental data (left-hand scale) in according to Eq. (54).

The calculated frequency dependences of the transmittance for Au and Ag thin films of different thicknesses are compared with the experimental data in Fig. 5. When comparing the results of our calculations with experimental data, it is necessary to take into consideration that our definition of the transmittance is different from that which is normally used by experimentalists.

In the transmittance, Eq. (20), the value I is the same in both cases: This is an intensity of radiation, which comes out from the film through the surface $x=L/2$. Experimentalists take I_0 as intensity of radiation incident onto the surface of the film $x=-L/2$. Of course, certain fraction of the radiation penetrates inside while the remaining part is reflected. We do not consider reflection and assume I_0 to be intensity of radiation, which *comes into the film* through the surface $x=-L/2$. To make a comparison with the theory, experimental values of the transmittance TR_{exp} are recalculated by using the formula

$$\mathrm{TR} = \frac{\mathrm{TR}_{\mathrm{exp}}}{1-R}, \tag{54}$$

where R is the value of reflection coefficient obtained by measuring under the same conditions as $\mathrm{TR}_{\mathrm{exp}}$.[4,5] The results of the recalculation are also presented in Fig. 5.

The absorbance η is determined by the functions Im $\epsilon(\hbar\omega)$ and Re $\epsilon(\hbar\omega)$ according to expression (22). The frequency dependences of these functions exhibit a different behavior (Fig. 6).

Unlike the function Im $\epsilon(\hbar\omega)$, the function Re $\epsilon(\hbar\omega)$ has not only pronounced resonance maxima but also minima shown as inverted peaks. The height of both peaks increases with an increase in the frequency, so that, eventually, one of the inverted peaks intersects the abscissa axis, and the function Re $\epsilon(\hbar\omega)$ becomes negative [in contrast to the function Im $\epsilon(\hbar\omega)$ that is always positive in sign]. The minimum transmittance should be identified with the minimum of the function Re $\epsilon(\hbar\omega)$, which is located in the vicinity of the frequency $\hbar\omega_{\max}=\hbar\omega_0(2m_{\mathrm{F}}+1)$.

At frequencies $\hbar\omega > \hbar\omega_{\max}$, the absorbance is determined only by the real part of the dielectric function: $\eta \approx (2\omega/c)\sqrt{|\mathrm{Re}\ \epsilon|}$. It is easy to check that the absorbance tends to a specific constant value with an increase in the frequency. The transmittance TR, Eq. (21), is characterized by the same tendency. This tendency can be clearly seen in Fig. 5. The peaks associated with the transitions between far subbands are clearly distinguished against the background of the monotonic increase in the transmittance. In particular, the transition $m_{\mathrm{F}}-3 \rightarrow m_{\mathrm{F}}$ manifests itself at $\hbar\omega \approx 1.8$ eV ($L=4$ nm).

To the zero order in L/λ, diagonal components of the dielectric tensor only are not equal to zero. Solid lines in Fig. 5 represent transmittance computed by Eqs. (21) and (22) using ϵ_{xx}. The transmittance indicates a change in a normal to surface component of an electric field of a wave passed through a film. It is this component that causes optical transitions between subbands formed by the size quantization. Dashed lines represent transmittance calculated with using ϵ_{zz} ($\epsilon_{zz}=\epsilon_{yy}$) which shows a weakening of a parallel to surface component of an electric field. Such a transmittance is observed at normal incidence of radiation onto a film.

In the region $\hbar\omega > \hbar\omega_{\max}$, a mechanism of dissipation (i.e., value of the relaxation time τ) affects the transmittance weakly. Dissipation manifests itself noticeably only in vicinity of the minimum of transmittance. Thus, discrepancies between theory and experiment at these frequencies could not be explained by either a mechanism of dissipation or an orientation of a film in field. A remarkable feature, as seen from Fig. 5, is a noticeable exceeding of measured transmittance over computed one (except of the last section, where there is a good agreement). This implies that the discrepancy between the theory and experiment can be attributed to a large nonhomogeneity in thickness and especially an absence of continuity, i.e., it can be explained by the presence of regions of a substrate without coating.

Let us name the ratio of coating area to substrate area by the coating coefficient p and denote coating thickness as L'. The mean thickness which is usually determined by experimentalists from the mass of a film and substrate area is $L=pL'$. Transmittance of a "holey" film of thickness L is

$$\mathrm{TR}(L) = 1-p+p\mathrm{TR}(L') = 1-p+p\mathrm{TR}(L/p).$$

Reducing p, it is possible to increase transmittance up to 1. For example, transmittance of a film with thickness $L=4$ nm and coating coefficient $p=0.45$ at the frequency $\hbar\omega=1$ eV is equal to 0.75, i.e., discrepancy with the experimental value is twice lowered (see Fig. 5).

In the frequency region $\hbar\omega < 0.5$ eV, there are experimental data for transmittance of thin films of Au (Ref. 9) and Pb.[9,14] Unfortunately data for reflection are absent hence the recalculation of experimental results like that represented above is impossible. However, taking into account that this recalculation leads to an increase in transmittance value, we guess experimental data for Au (Ref. 9) to be in agreement with our calculations under assumption of a normal incidence of radiation onto a film (Fig. 5). Moreover, the recalculation can change a type of dependence on frequency for transmittance, i.e., a rising can be replaced by a falling after the recalculation (see Fig. 5 for Au, $L=5.8$ nm). This could explain why within frequency interval (0.2,0.5 eV) dependence of transmittance on frequency is decreasing or absent at all according to our calculations whereas an increasing is observed in experiment.[14] As to value of transmittance for Pb films, it is difficult to compare calculations with experimental data because results of different experiments vary essentially. Thus transmittance value for Pb film of 4 nm thickness is given in Ref. 9 as 0.79 at 0.05 eV but it is 0.12 only at the close frequency 0.12 eV following[14] (in addition, transmittance diverges in value 1.5 times for different technologies of film coating[14]).

C. Wire

The frequency dependences of Re σ_{xx} and Im σ_{xx} for the Au wire of diameter 1.6 nm are presented in Fig. 7. For such a small diameter, the peaks corresponding to the transitions between levels of the size quantization (subbands) manifest itself clearly. In spite of the rather complete spectrum k_{mn}, position of the peaks is well predicted.

Let us find, for example, the position of the peak in Re σ_{xx} which has the maximum height. The height of the peaks is proportional to $|\langle m+1,n'|\hat{p}_x|mn\rangle|^2\Sigma_p 1$. The matrix element has the maximum magnitude at $n'=n$ because under this condition the integral in Eq. (38) takes on the maximum value. Further, by using Eqs. (52) and (53), it is easy to determine that the maximum height is realized at $m=0$, $n'=n=n_{\mathrm{F}}$. For the diameter $d=1.6$ nm, the number $n_{\mathrm{F}} \approx k_{\mathrm{F}}^0\rho_0/\pi$ is equal to 3. As a result we have

$$\hbar\omega_{\max} = \frac{\hbar^2(k_{1,3}^2-k_{0,3}^2)}{2m_e} = \frac{\hbar^2(a_{1,3}^2-a_{0,3}^2)}{2m_e\rho_0^2} = 1.40\ \mathrm{eV}.$$

This is in good agreement with numerical calculations presented in Fig. 7. The height of the peaks in Fig. 7 also confirms our estimation.

Figure 7 demonstrates the important fact Re $\sigma_{xx} > 0$ over

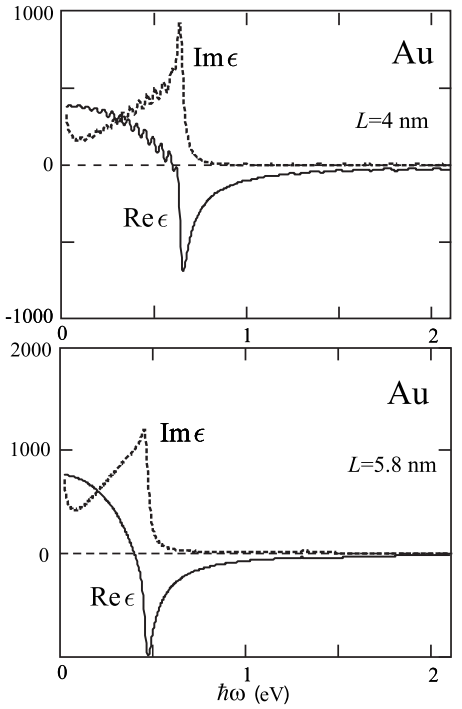

FIG. 6. Frequency dependences of the real and imaginary parts of the film dielectric function calculated by Eq. (16).

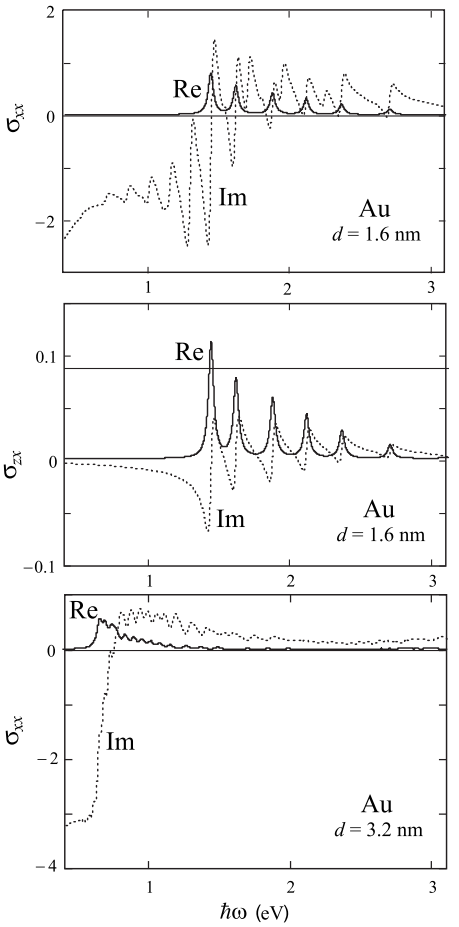

FIG. 7. Calculated frequency dependences of the real and imaginary parts of $\sigma_{\alpha\beta}$ (in $e^2/2a_0\hbar$ units) for Au wires of various diameter d.

all frequency range. In contrast to this, Im σ_{xx} is a variable in sign function of the frequency. The frequency dependences of Re σ_{zx} and Im σ_{zx} are also presented in Fig. 7. As it was expected, the position of the peaks is identical both for Re σ_{zx} and Im σ_{zx} but the height is one order smaller in the first case.

Comparing the upper and lower parts of Fig. 7, we can trace the size dependence of the conductivity for ultrathin metal wires. When d increases, the peaks shift to the left with displacement equal to $\Delta\omega=\omega'-\omega=\omega(\rho_0^2/\rho_0'^2-1)$. More distant peaks (with lager value ω) have lager displacement so that the interval occupied by the peaks contracts. At the same time, new peaks appear within this interval because with enlarging ρ_0 the number of levels and the number of the possible transitions between them increase. Distance between peaks decreases, and when it approaches $\hbar/\tau$, the peaks begin to merge together.

It is interesting to compare results of the study for the optical conductivity of ultrathin metal wires with analogous results for ultrathin films. Divergences are associated with the different dimensionality of the systems. This is reflected in an essential difference in the energetic spectra and also in the fact that after calculation of quasicontinuous states, in the case of a wire, the summation over two numbers m, n remains, while in the case of a film, it remains over one number only (which numerates values of the x component of the electron momentum). It is this fact that explains approximately one order lower height of the maximum in the frequency dependence of the conductivity of a wire compared to the case of a film. Indeed,

$$\frac{\mathrm{Re}\ \sigma_{xx}^{\mathrm{wire}}}{\mathrm{Re}\ \sigma_{xx}^{\mathrm{film}}} \cong \frac{\Omega_{\mathrm{wire}}^{-1}\sum_{p} 1}{\Omega_{\mathrm{film}}^{-1}\sum_{p,n} 1} = \frac{2\mathcal{L}}{\pi}\frac{\sqrt{(k_{\mathrm{F}}^{\mathrm{wire}})^2-k_{0n_{\mathrm{F}}}^2}}{\pi\rho_0^2\mathcal{L}}\left\{\frac{ab}{\pi^2}\frac{\pi\{(k_{\mathrm{F}}^{\mathrm{film}})^2-k_{m\mathrm{F}}^2\}}{abL}\right\}^{-1} \cong \frac{10^{-1}}{\sqrt{\rho_0\ [\mathrm{nm}]}}\frac{L^2}{\rho_0^2}$$

because

$$(k_{\mathrm{F}}^{\mathrm{wire}})^2-k_{0n_{\mathrm{F}}}^2 \cong 2\pi k_{\mathrm{F}}^0/\rho_0, \quad (k_{\mathrm{F}}^{\mathrm{film}})^2-k_{m_{\mathrm{F}}}^2 \cong 2\pi k_{\mathrm{F}}^0/L.$$

For L, $\rho_0 \cong 1$ nm we obtain Re $\sigma_{xx}^{\mathrm{wire}}$/Re $\sigma_{xx}^{\mathrm{film}} \cong 10^{-1}$.

As to the different position of the peaks, this may be completely explained by characteristic properties of spectra of the 1D and 2D systems.

The frequency dependences of Re σ_{xx} for the Al and Pb wires of diameter 1.6 nm are presented in Fig. 8. It is surprising that peaks in the conductivity of the Pb wire are absolutely absent. The reason of this is a small value of the relaxation time for Pb equal to $\tau=1.4\times10^{-15}$ s so that width

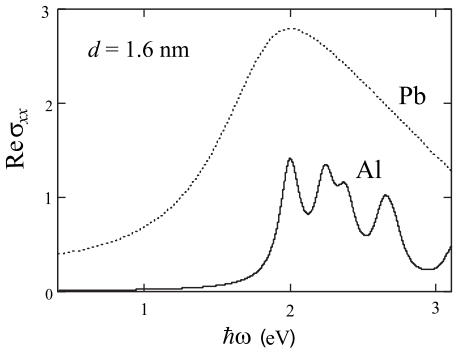

FIG. 8. Calculated frequency dependences of the real part of σ_{xx} (in $e^2/2a_0\hbar$ units) for Al and Pb wires.

of the peaks $\hbar/\tau=0.44$ eV. In this respect, Al, with $\hbar/\tau=0.08$ eV, holds an intermediate position between Au and Pb. For calculations we use values of the relaxation time for bulk metals taken from.[35]

In spite of an absence of peaks in the frequency dependence of the conductivity for the Pb wire, its maximum may be found in such a way as the position of the maximum height peak in the conductivity of the Au wire was determined above, with the difference that this time $n_F=4$,

$$\hbar\omega_{\max}=\frac{\hbar^2(a_{1,4}^2-a_{0,4}^2)}{2m_e\rho_0^2}=2.1\ \text{eV}.$$

This value agrees well with Fig. 8 taking into account the large width of the peaks.

Surprisingly, the difference in the obtained results for Al and Pb (due to the different values of τ) indicate size-frequency dependences, which can be expected for films and wires, inhomogeneous in thickness considered, for example, in Refs. 40–44. If fluctuations of sizes in 1D and 2D systems lead to a strong effective reduction in τ, experimental size dependences of conductivity are noticeably smoothed irrespective of a metal kind. We will devote select publication to the theory of transport in films and wires with rough surface.

VI. CONCLUSIONS

The conductivity tensor is introduced for the low-dimensional electron systems. Components of the conductivity tensor for a quasihomogeneous ultrathin metal film and wire are calculated within the particle-in-a-box model on the assumption that the component of the induced current with the wave vector equal to the wave vector of the electromagnetic field is dominating.

Over infrared region the condition qL, $q\rho_0\ll 1$ is satisfied allowing us to express components of the conductivity tensor in terms of the according small value. All nondiagonal components of the conductivity tensor are equal to zero in zero order of the expansion. They appear in linear approximation. The important fact that the real part of the diagonal components is non-negative over all frequency range, with the guarantee $Q>0$ for the dissipation of energy, is proved.

As a result of comparing the according components of the conductivity tensor for a film and a wire of the same thickness of order 1 nm, one order smaller value for a wire is obtained. In such a manner different density of states near the Fermi level manifests itself (it is greater for a film). It is found that the discrepancy between our results and the theory[22] increases and becomes substantial, as the characteristic small dimension of the system decreases. This discrepancy is associated with the strong dependence of the Fermi level on this dimension for small values of order of the Fermi wavelength. This size dependence of the Fermi level has an oscillatory form. Transmittance is calculated for a simple, well-defined model without fitting parameters.

ACKNOWLEDGMENTS

We are grateful to A. V. Babich and A. V. Korotun for help in the calculations and to W. V. Pogosov for reading the manuscript. This work was supported by the Ministry of Education and Science of Ukraine.

APPENDIX: THE MATRIX ELEMENTS

The expressions for momentum projections in cylindrical coordinates have a form

$$\hat{p}_z=-i_0\hbar\frac{\partial}{\partial z},$$

$$\hat{p}_x=-i_0\hbar\left\{\cos\varphi\frac{\partial}{\partial\rho}-\frac{\sin\varphi}{\rho}\frac{\partial}{\partial\varphi}\right\},$$

$$\hat{p}_y=-i_0\hbar\left\{\sin\varphi\frac{\partial}{\partial\rho}+\frac{\cos\varphi}{\rho}\frac{\partial}{\partial\varphi}\right\}. \tag{A1}$$

Using Eqs. (23)–(28) and (A1), we have

$$\begin{aligned}\langle j|\hat{p}_x|i\rangle=&-i_0\frac{\hbar}{2}\delta_{pp'}\left\{\frac{1}{2\pi}\int_0^{2\pi}(e^{-im'\varphi}e^{i(m-1)\varphi}\right.\\&+e^{-im'\varphi}e^{i(m+1)\varphi})d\varphi\int_0^{\rho_0}R_{m'n'}\frac{dR_{mn}}{d\rho}\rho d\rho\\&+\frac{m}{2\pi}\int_0^{2\pi}(e^{-im'\varphi}e^{i(m-1)\varphi}\\&\left.-e^{-im'\varphi}e^{i(m+1)\varphi})d\varphi\int_0^{\rho_0}R_{m'n'}R_{mn}d\rho\right\}\\=&-i_0\frac{\hbar}{2}\delta_{pp'}\left\{\delta_{m-1,m'}\left(\int_0^{\rho_0}R_{m'n'}\frac{dR_{mn}}{d\rho}\rho d\rho\right.\right.\\&\left.+m\int_0^{\rho_0}R_{m'n'}R_{mn}d\rho\right)\\&+\delta_{m+1,m'}\left(\int_0^{\rho_0}R_{m'n'}\frac{dR_{mn}}{d\rho}\rho d\rho\right.\\&\left.\left.-m\int_0^{\rho_0}R_{m'n'}R_{mn}d\rho\right)\right\}.\end{aligned} \tag{A2}$$

Then using relation $I'_m(x) = \pm mI_m(x)/x \mp I_{m\pm1}(x)$ from Ref. 38, we obtain Eqs. (37) and (38).

In a similar way we find

$$\begin{aligned}\langle j|x\hat{p}_z|i\rangle &= -i_0\hbar \int\int\int \left\{ R_{m'n'}\Phi^*_{m'}Z^*_{p'}(\rho\cos\varphi)R_{mn}\Phi_m \frac{dZ_p}{dz} \right\} \\ &\quad \times \rho d\rho d\varphi dz \\ &= \hbar k_{zp}\delta_{pp'} \int_0^{2\pi} \Phi^*_{m'}\Phi_m \cos\varphi d\varphi \int_0^{\rho_0} R_{m'n'}R_{mn}\rho^2 d\rho \\ &= \frac{1}{2}\hbar k_{zp}\delta_{pp'}(\delta_{m-1,m'} + \delta_{m+1,m'}) \int_0^{\rho_0} R_{m'n'}R_{mn}\rho^2 d\rho \\ &= \frac{1}{2}\hbar k_{zp}\delta_{pp'}\left(\delta_{m-1,m'} \int_0^{\rho_0} R_{m-1,n'}R_{mn}\rho^2 d\rho \right. \\ &\quad \left. + \delta_{m+1,m'} \int_0^{\rho_0} R_{m+1,n'}R_{mn}\rho^2 d\rho \right). \end{aligned} \tag{A3}$$

*Corresponding author; vpogosov@zntu.edu.ua

[1] R. D. Fedorovich, A. G. Naumovets, and P. M. Tomchuk, Phys. Rep. **328**, 73 (2000).
[2] R. Otero, A. L. Vazquez de Parga, and R. Miranda, Phys. Rev. B **66**, 115401 (2002).
[3] A. Gloskovskii, D. A. Valdaitsev, M. Cinchetti, S. A. Nepijko, J. Lange, M. Aeschlimann, M. Bauer, M. Klimenkov, L. V. Viduta, P. M. Tomchuk, and G. Schönhense, Phys. Rev. B **77**, 195427 (2008).
[4] J. P. Gasparini and R. Fraisse, Thin Solid Films **30**, 111 (1975).
[5] J. Dryzek and A. Czapla, Phys. Rev. Lett. **58**, 721 (1987).
[6] D. A. Evans, M. Alonso, R. Cimino, and K. Horn, Phys. Rev. Lett. **70**, 3483 (1993).
[7] P. F. Henning, C. C. Homes, S. Maslov, G. L. Carr, D. N. Basov, B. Nikolić, and M. Strongin, Phys. Rev. Lett. **83**, 4880 (1999).
[8] G. Fahsold, A. Bartel, O. Krauth, N. Magg, and A. Pucci, Phys. Rev. B **61**, 14108 (2000).
[9] J. J. Tu, C. C. Homes, and M. Strongin, Phys. Rev. Lett. **90**, 017402 (2003).
[10] G. Fahsold, A. Priebe, N. Magg, and A. Pucci, Thin Solid Films **428**, 107 (2003).
[11] N. Bonod, S. Enoch, L. Li, E. Popov, and M. Neviere, Opt. Express **11**, 482 (2003).
[12] I. Vilfan and H. Phur, Eur. Phys. J. B **36**, 281 (2003).
[13] S. Ding, X. Wang, D. J. Chen, and Q. Q. Wang, Opt. Express **14**, 1541 (2006).
[14] A. Pucci, F. Kost, G. Fahsold, and M. Jałochowski, Phys. Rev. B **74**, 025428 (2006).
[15] M. C. Tringides, M. Jałochowski, and E. Bauer, Phys. Today **60**, 50 (2007).
[16] F. Neubrech, T. Kolb, R. Lovrincic, G. Fahsold, A. Pucci, J. Aizpurua, T. W. Cornelius, M. E. Toimil-Molares, R. Neumann, and S. Karim, Appl. Phys. Lett. **89**, 253104 (2006).
[17] O. L. Muskens, V. Giannini, J. A. Sanchez-Gil, and J. Gomez Rivas, Nano Lett. **7**, 2871 (2007).
[18] M. Klevenz, F. Neubrech, R. Lovrincic, M. Jałochowski, and A. Pucci, Appl. Phys. Lett. **92**, 133116 (2008).
[19] V. V. Pogosov, *Introduction to the Physics of Charge and Size Effects: Surface, Clusters, and Low-Dimensional Systems* (Fizmatlit, Moscow, 2006) (in Russian).
[20] V. V. Pogosov and E. V. Vasyutin, Nanotechnology **17**, 3366 (2006).
[21] L. D. Landau and E. M. Lifshits, *Elecrodynamics of Continuum Media* (Fizmatlit, Moscow, 2001) (in Russian).
[22] D. M. Wood and N. W. Ashcroft, Phys. Rev. B **25**, 6255 (1982).
[23] V. B. Sandomirskii, Sov. Phys. JETP **25**, 101 (1967).
[24] F. K. Schulte, Surf. Sci. **55**, 427 (1976).
[25] W. Ekardt, Phys. Rev. B **29**, 1558 (1984).
[26] P. J. Feibelman and D. R. Hamann, Phys. Rev. B **29**, 6463 (1984).
[27] J. C. Boettger, Phys. Rev. B **53**, 13133 (1996).
[28] A. Kiejna, J. Peisert, and P. Scharoch, Surf. Sci. **54**, 432 (1999).
[29] N. Zabala, M. J. Puska, and R. M. Nieminen, Phys. Rev. B **59**, 12652 (1999).
[30] I. Sarria, C. Henriques, C. Fiolhais, and J. M. Pitarke, Phys. Rev. B **62**, 1699 (2000).
[31] E. Ogando, N. Zabala, and M. J. Puska, Nanotechnology **13**, 363 (2002).
[32] V. V. Pogosov, V. P. Kurbatsky, and E. V. Vasyutin, Phys. Rev. B **71**, 195410 (2005).
[33] C. M. Horowitz, C. R. Proetto, and J. M. Pitarke, Phys. Rev. B **78**, 085126 (2008).
[34] Y. Han and D.-J. Liu, Phys. Rev. B **80**, 155404 (2009).
[35] N. Ashcroft and N. Mermin, *Solid State Physics* (Holt, Rinehart, and Winston, New York, 1976).
[36] N. D. Mermin, Phys. Rev. B **1**, 2362 (1970).
[37] G. A. Korn and T. M. Korn, *Mathematical Handbook for Scientists and Engineers*, 2nd ed. (Dover, New York, 2000).
[38] I. S. Gradshteyn and I. M. Ryzhik, *Table of Integrals, Series and Products*, 5th ed. (Academic Press, San Diego, 1994).
[39] J. M. Ziman, *Principles of the Theory of Solids* (Cambridge University Press, New York, 1972).
[40] Z. Tešanović, M. V. Jarić, and S. Maekawa, Phys. Rev. Lett. **57**, 2760 (1986).
[41] N. Trivedi and N. W. Ashcroft, Phys. Rev. B **38**, 12298 (1988).
[42] G. Fishman and D. Calecki, Phys. Rev. Lett. **62**, 1302 (1989); Phys. Rev. B **43**, 11581 (1991).
[43] A. E. Meyerovich and I. V. Ponomarev, Phys. Rev. B **65**, 155413 (2002).
[44] Y. Cheng and A. E. Meyerovich, Phys. Rev. B **73**, 085404 (2006).